AIP | The Journal of Chemical Physics

Full-dimensional quantum dynamics of CO in collision with H2

Benhui Yang, N. Balakrishnan, P. Zhang, X. Wang, J. M. Bowman, R. C. Forrey, and P. C. Stancil

Citation: The Journal of Chemical Physics **145**, 034308 (2016); doi: 10.1063/1.4958951
View online: http://dx.doi.org/10.1063/1.4958951
View Table of Contents: http://scitation.aip.org/content/aip/journal/jcp/145/3?ver=pdfcov
Published by the AIP Publishing

Articles you may be interested in

A full-dimensional quantum dynamical study of H2+H2 collisions: Coupled-states versus close-coupling formulation
J. Chem. Phys. **140**, 064308 (2014); 10.1063/1.4864357

Vibration-vibration and vibration-translation energy transfer in H2-H2 collisions: A critical test of experiment with full-dimensional quantum dynamics
J. Chem. Phys. **138**, 104302 (2013); 10.1063/1.4793472

Full-dimensional quantum dynamics calculations of H2–H2 collisions
J. Chem. Phys. **134**, 014301 (2011); 10.1063/1.3511699

Quantum scattering of SiS with H 2 : Potential energy surface and rate coefficients at low temperature
J. Chem. Phys. **128**, 034306 (2008); 10.1063/1.2820770

Full-dimensional quantum wave packet study of rotationally inelastic transitions in H 2 + H 2 collision
J. Chem. Phys. **117**, 5183 (2002); 10.1063/1.1500731

Reuse of AIP Publishing content is subject to the terms: https://publishing.aip.org/authors/rights-and-permissions. Downloaded to IP: 128.118.81.59 On: Wed, 23 Nov 2016 20:49:22

Full-dimensional quantum dynamics of CO in collision with H_2

Benhui Yang,[1] N. Balakrishnan,[2] P. Zhang,[3] X. Wang,[4] J. M. Bowman,[4] R. C. Forrey,[5] and P. C. Stancil[1]

[1]*Department of Physics and Astronomy and the Center for Simulational Physics, The University of Georgia, Athens, Georgia 30602, USA*
[2]*Department of Chemistry, University of Nevada, Las Vegas, Nevada 89154, USA*
[3]*Department of Chemistry, Duke University, Durham, North Carolina 27708, USA*
[4]*Department of Chemistry, Emory University, Atlanta, Georgia 30322, USA*
[5]*Department of Physics, Penn State University, Berks Campus, Reading, Pennsylvania 19610, USA*

(Received 16 December 2015; accepted 3 July 2016; published online 21 July 2016)

Inelastic scattering computations are presented for collisions of vibrationally and rotationally excited CO with H_2 in full dimension. The computations utilize a newly developed six-dimensional potential energy surface (PES) and the previously reported four-dimensional V12 PES [P. Jankowski *et al.*, J. Chem. Phys. **138**, 084307 (2013)] and incorporate full angular-momentum coupling. At low collision energies, pure rotational excitation cross sections of CO by *para*-, *ortho*-, and *normal*-H_2 are calculated and convolved to compare with recent measurements. Good agreement with the measured data is shown except for $j_1 = 0 \rightarrow 1$ excitation of CO for very low-energy *para*-H_2 collisions. Rovibrational quenching results are presented for initially excited CO($v_1 j_1$) levels with $v_1 = 1$, $j_1 = 1$–5 and $v_1 = 2$, $j_1 = 0$ for collisions with *para*-$H_2(v_2 = 0, j_2 = 0)$ and *ortho*-$H_2(v_2 = 0, j_2 = 1)$ over the kinetic energy range 0.1–1000 cm^{-1}. The total quenching cross sections are found to have similar magnitudes, but increase (decrease) with j_1 for collision energies above ~300 cm^{-1} (below ~10 cm^{-1}). Only minor differences are found between *para*- and *ortho*-H_2 colliders for rovibrational and pure rotational transitions, except at very low collision energies. Likewise, pure rotational deexcitation of CO yields similar cross sections for the $v_1 = 0$ and $v_1 = 1$ vibrational levels, while rovibrational quenching from $v_1 = 2, j_1 = 0$ is a factor of ~5 larger than that from $v_1 = 1, j_1 = 0$. Details on the PES, computed at the CCSD(T)/aug-cc-pV5Z level, and fitted with an invariant polynomial method, are also presented. *Published by AIP Publishing.* [http://dx.doi.org/10.1063/1.4958951]

I. INTRODUCTION

Over many decades much effort has been devoted to theoretical quantum mechanical studies of diatom-diatom inelastic collisions with significant advances resulting from numerical algorithm development and increases in computational processing power. However, full-dimensional (6D) studies of diatom-diatom systems have been limited to H_2–H_2 collisions. These studies have included both time-independent[1] and time-dependent[2] approaches for solving the Schrödinger equation. Moreover, to make these computations practical, various angular-momentum decoupling approximations have been invoked. To assess the usefulness of such approximations, it is desirable to develop accurate computational methods which are capable of handling large-scale calculations for diatom-diatom (and larger) scattering without resorting to such approximations. Indeed, the first numerically exact 6D close-coupling (CC) computations of rovibrational transitions in the $H_2 + H_2$ system were reported recently.[3–5] Subsequently, Yang *et al.*[6] reported full-dimensional CC calculations of the $CO + H_2$ system on a 6D potential energy surface (PES) derived from high-level *ab initio* calculations.

From a theoretical point of view, the development of exact quantum close-coupling methods for molecule-molecule and other polyatomic systems seem viable, but due to the large number of internal states of the molecules involved, their numerical implementation is currently not feasible for systems with more than four atoms. This difficulty has been alleviated to some extent by using angular momentum decoupling schemes, for example, the coupled-states (CS) approximation performed recently by Forrey *et al.*,[7,8] which has been successfully implemented in $H_2 + H_2$ and $CO + H_2$ rovibrational scattering calculations and achieved reasonable agreement with CC results.

Rovibrational collision of CO with H_2 is an important process in a variety of astrophysical environments including interstellar clouds and photodissociation regions. The collisional rate coefficients are crucial to astrophysical modeling, but are difficult to measure, and therefore are mostly obtained from theory. Though great progress has been made in experimental[9–20] and theoretical[6,21–41] studies of $CO + H_2$ structure and dynamics, there is still a lack of a comprehensive set of state-to-state rovibrational cross sections and rate coefficients for $CO + H_2$ that are required for astrophysical modeling.

Since the close-coupling calculations of $CO + H_2$ rate coefficients by Green[21] using an approximate PES, a number of PESs have been constructed for the $CO + H_2$ complex.[6,25,26,32,35–37] Specifically, Jankowski and coworkers reported three accurate four-dimensional (4D) rigid-rotor PESs.[35–37] These 4D PESs were calculated on four-, five-, and six-dimensional (6D) grids using high level electronic

Reuse of AIP Publishing content is subject to the terms: https://publishing.aip.org/authors/rights-and-permissions. Downloaded to IP: 128.118.81.59 On: Wed, 23 Nov 2016 20:49:22

structure theory, followed by averaging over the ground intramolecular vibrations of CO and H_2. Comparative studies of collisional cross sections and rate coefficients using the three PESs have been presented in our earlier work[6,40,41] and by other authors.[19,20,33,39]

Taking into account the CO vibrational mode, Schinke and co-workers[25,26] extended the rigid-rotor CO + H_2 PES[24] to include dependence on CO bond distances and made it available to study vibrationally inelastic processes of CO. This surface was adopted by Bačić *et al.*[25,26] and Reid *et al.*[30] to investigate the vibrational deactivation of CO ($v = 1$) by inelastic collisions with H_2. However the dynamical calculations of Bačić *et al.* and Reid *et al.* were performed using the infinite order sudden (IOS) and coupled-states (CS) approximations, respectively. The IOS approximation eliminates the rotational channel coupling and neglects the internal rotation. As a result, rotational state-to-state transitions cannot be resolved dynamically. Another 4D *ab initio* PES including the CO vibrational coordinate dependence was presented by Kobayashi *et al.*[32] Using this potential and the CC method, Flower[34] calculated cross sections for the rovibrational excitation of CO in collision with H_2.

Most recently, Yang *et al.*[6] presented a high-level 6D interaction potential surface based on nearly 400 000 geometries fitted with an invariant polynomial approach.[42] The 6D PES is a significant step forward in quantitative modeling of the CO + H_2 complex. Using this PES, the first essentially exact full-dimensional dynamics computations for inelastic rovibrational quenching of CO from $v_1 = 1, j_1 = 0$ due to H_2 impact were performed. These dynamics calculations were performed within a full angular-momentum-coupling formulation, representing one of the largest such computations performed to date. Agreement with experimentally determined integral cross sections and rate coefficients was obtained for both rotational and vibrational transitions, confirming the accuracy of the 6D PES and scattering calculations. In this paper, we extend our previous $v_1 = 1, j_1 = 0$ rovibrational scattering calculations to higher CO rotational states and to $v_1 = 2$. Further details on the 6D PES are also presented.

The rest of the paper is organized as follows. Sec. II briefly describes the theoretical methods. The results are presented and discussed in Sec. III, and Section IV summarizes the results, discusses the astrophysical applications, and presents an outlook on future work.

II. THEORETICAL METHODS

In this section, we will briefly describe the methods we used in the potential energy surface calculation and fit and rovibrational inelastic scattering calculations. The reader is referred to Refs. 3, 6, and 42 for more detailed discussions of the methodology. Atomic units are used throughout unless otherwise noted.

A. Potential energy surface computations and fit

The electronic ground state interaction potential of CO + H_2 was computed on a six-dimensional (6D) grid using

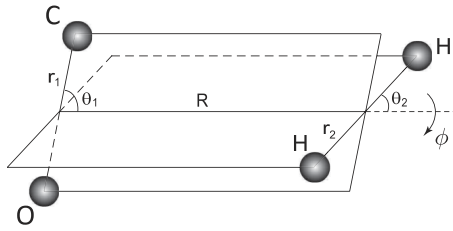

FIG. 1. The six-dimensional Jacobi coordinates for the CO–H_2 system.

Jacobi coordinates $(R, r_1, r_2, \theta_1, \theta_2, \phi)$ as shown in Fig. 1. R is the center-of-mass distance between CO and H_2. r_1 and r_2 represent the bond lengths describing the vibration of CO and H_2, respectively. θ_1 (θ_2) is the in-plane orientation angle between $\vec{r}_1$ ($\vec{r}_2$) and $\vec{R}$, and ϕ the out-of-plane dihedral angle. In the computations of the potential energy surface, R spans from 4.0 to 18.0 a_0 and the bond distances are taken over the ranges $1.7359 \le r_1 \le 2.5359$ a_0 and $1.01 \le r_2 \le 1.81$ a_0, which support vibrational states of CO up to $v_1 = 5$ and H_2 $v_2 = 0$ in the scattering calculations. All angular coordinates were computed with $0° \le \theta_1 \le 360°$ and $0° \le \theta_2, \phi \le 180°$.

The electronic structure calculations were performed with MOLPRO2010.1.[43] Potential energies were computed using the explicitly correlated coupled-cluster (CCSD(T)-F12B) method[44,45] and cc-pcvqz-f12 orbital basis sets[46] at all of the configurations. Benchmark calculations at the CCSD(T)-F12b/cc-pcvqz-f12 level were carried out on selected molecular configurations and results were compared with those from the conventional CCSD(T) method using aug-cc-pV5Z and aug-cc-pV6Z basis sets. The counter-poise (CP)[47] corrected interaction energy agrees closely with those derived from CCSD(T)/aug-cc-pV6Z. The interaction potential energy surface was corrected for basis set superposition error (BSSE).[48]

To fit the CO–H_2 interaction potential in 6D (referred to as V6D), an invariant polynomial method[42] was used. The potential was expressed in terms of Morse-type variables, $y_i = e^{-0.5 d_i}$,

$$V(y_1 \cdots y_6) = \sum_{n_1 \cdots n_6}^{N} c_{n_1 \cdots n_6} y_1^{n_1} y_6^{n_6} \times [y_2^{n_2} y_3^{n_3} y_4^{n_4} y_5^{n_5} + y_2^{n_5} y_3^{n_4} y_4^{n_3} y_5^{n_2}], \quad (1)$$

where d_i are the internuclear distances between two atoms, $d_1 = d_{HH'}$, $d_2 = d_{OH'}$, $d_3 = d_{CH'}$, $d_4 = d_{CH}$, $d_5 = d_{OH}$, and $d_6 = d_{CO}$. The order of the polynomials, n_i, $i = 1 - 6$ ranges from 0-6 with the total power of the polynomial, $N = \sum_{i=1}^{6} n_i$, restricted to a maximum value of 6. Expansion coefficients $c_{n_1 \cdots n_6}$ were determined by a weighted linear least-squares fit to the *ab initio* electronic potential energies up to a maximum of 10 000 cm^{-1}.

Some details of the fitted interaction PES were illustrated in Ref. 6. Fig. 2 shows the V6D interaction PES near the global minimum, which corresponds to the collinear arrangement H–H–C–O ($\theta_1 = 0, \theta_2 = 0, \phi = 0$) with a depth of -85.937 cm^{-1} at $R = 8.0$ a_0. Fig. 3 depicts the anisotropy of the V6D and V12 PESs in θ_1, θ_2, and ϕ,

Reuse of AIP Publishing content is subject to the terms: https://publishing.aip.org/authors/rights-and-permissions. Downloaded to IP: 128.118.81.59 On: Wed, 23 Nov 2016 20:49:22

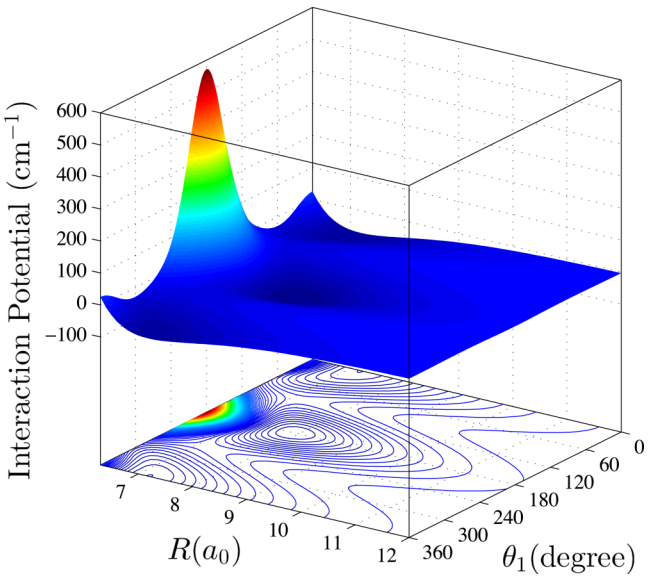

FIG. 2. The CO–H_2 interaction potential energy surface V6D as a function of R and θ_1 with $\theta_2 = 0$, $\phi = 0$, $r_1 = r_e(\mathrm{CO}) = 2.1359$ a_0, and $r_2 = r_e(\mathrm{H_2}) = 1.4011$ a_0. Note that the CO(r_1) and $H_2(r_2)$ diatom potentials have been subtracted as given by Eq. (3).

respectively. θ_1 describes the orientation of CO, and the anisotropy with respect to θ_1 is the largest because of the larger CO bond length. V6D and V12 PESs show similar behavior; however, some differences can be seen which may partly be attributed to the fact that V6D is a full-dimensional surface, while V12 is a vibrationally averaged 4D surface.

B. Scattering theory and computational details

The quantum CC formalism for molecular collisions was first developed in 1960 by Arthurs and Dalgarno[49] for a rigid-rotor scattered by a spherical atom and subsequently extended to full vibrational motion to study diatom-diatom collisions by several authors.[50–53] The resulting coupled-channel equations, based on the time-independent Schrödinger equation, are solved numerically. In the 6D Jacobi coordinates shown in Fig. 1, the Hamiltonian of CO + H_2 can be written as

$$H(\vec{r}_1,\vec{r}_2,\vec{R}) = T(\vec{r}_1) + T(\vec{r}_2) + T(\vec{R}) + U(\vec{r}_1,\vec{r}_2,\vec{R}), \quad (2)$$

where the radial kinetic energy term $T(\vec{R})$ describes the center-of-mass motion of the scattering system, $T(\vec{r}_1)$ and $T(\vec{r}_2)$ are the kinetic energy terms for CO and H_2, respectively. $U(\vec{r}_1,\vec{r}_2,\vec{R})$ denotes the total potential energy surface and is given by

$$U(\vec{r}_1,\vec{r}_2,\vec{R}) = V(\vec{r}_1,\vec{r}_2,\vec{R}) + V_1(\vec{r}_1) + V_2(\vec{r}_2), \quad (3)$$

where $V(\vec{r}_1,\vec{r}_2,\vec{R})$ describes the interaction potential between CO and H_2 which vanishes when the two molecules are far apart.

To facilitate the scattering computations, $V(R,r_1,r_2,\theta_1,\theta_2,\phi)$ is expressed as

$$V(R,r_1,r_2,\theta_1,\theta_2,\phi) = \sum_{\lambda_1\lambda_2\lambda_{12}} A_{\lambda_1\lambda_2\lambda_{12}}(r_1,r_2,R) Y_{\lambda_1\lambda_2\lambda_{12}}(\hat{r}_1,\hat{r}_2,\hat{R}), \quad (4)$$

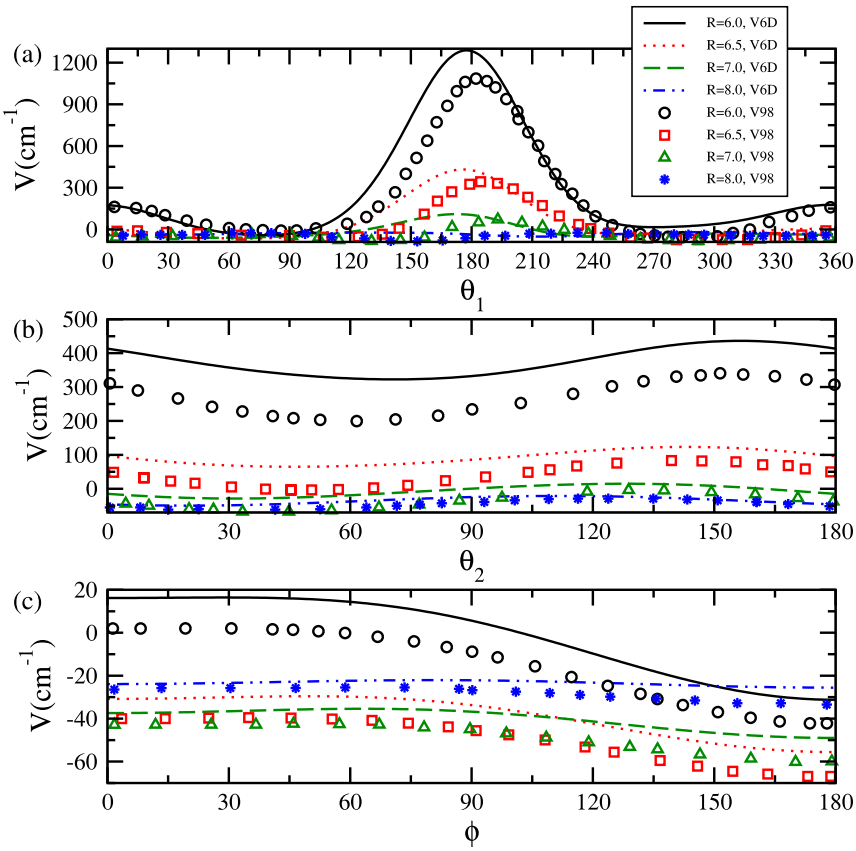

FIG. 3. Cut through the V6D PES at $R = 6.0$, 6.5, 7.0, and 8.0 a_0. $r_1 = 2.1359$ a_0, $r_2 = 1.4011$ a_0. (a) θ_1 dependence for $\theta_2 = 135°$ and $\phi = 0°$; (c) θ_2 dependence for $\theta_1 = 225°$ and $\phi = 135°$; (b) ϕ dependence for $\theta_1 = 270°$ and $\theta_2 = 135°$. Lines are for V6D PES and symbols are from Ref. 35 for the vibrationally averaged 4D V98 PES.

Reuse of AIP Publishing content is subject to the terms: https://publishing.aip.org/authors/rights-and-permissions. Downloaded to IP: 128.118.81.59 On: Wed, 23 Nov 2016 20:49:22

TABLE I. Parameters used in the scattering calculations.

	Basis set[a]	N_{θ_1}	N_{θ_2}	N_ϕ	N_{r_1}	N_{r_2}	λ_1	λ_2
CO ($v_1 = 1$)								
para-H_2–CO	[(0,22;1,20)(0,4)]	12	12	8	18	18	8	4
ortho-H_2–CO	[(0,22;1,20)(0,3)]	12	12	8	18	18	8	4
CO ($v_1 = 2$)								
para-H_2–CO	[(0,22;1,20;2,15)(0,4)]	12	12	8	18	18	8	4

[a]Basis set $[(v_1 = 0, j^{\max}_{v_1=0}; v_1 = 1, j^{\max}_{v_1=1})(v_2 = 0, j^{\max}_{v_2=0})]$ is presented by the maximum rotational quantum number $j^{\max}_{v_1}$ and $j^{\max}_{v_2}$ included in each relevant vibrational level v_1 and v_2 for CO and H_2, respectively.

with the bi-spherical harmonic function expressed as

$$Y_{\lambda_1\lambda_2\lambda_{12}}(\hat{r}_1, \hat{r}_2, \hat{R}) = \sum_{m_{\lambda_1} m_{\lambda_2} m_{\lambda_{12}}} \langle \lambda_1 m_{\lambda_1} \lambda_2 m_{\lambda_2} | \lambda_{12} m_{\lambda_{12}} \rangle \times Y_{\lambda_1 m_{\lambda_1}}(\hat{r}_1) Y_{\lambda_2 m_{\lambda_2}}(\hat{r}_2) Y^*_{\lambda_{12} m_{\lambda_{12}}}(\hat{R}), \quad (5)$$

where $0 \le \lambda_1 \le 8$, $0 \le \lambda_2 \le 4$ was adopted for the potential expansion in the scattering calculations. Only even values of λ_2 contribute due to the symmetry of H_2.

We use combined molecular state (CMS) notation, $(v_1 j_1 v_2 j_2)$, to describe a combination of rovibrational states for CO $(v_1 j_1)$ and H_2 $(v_2 j_2)$. v and j are the vibrational and rotational quantum numbers. A CMS represents a unique quantum state of the diatom–diatom system before or after a collision. The rovibrational state-to-state cross section as a function of collision energy E is given by

$$\sigma_{v_1 j_1 v_2 j_2 \to v_1' j_1' v_2' j_2'}(E) = \frac{\pi}{(2j_1+1)(2j_2+1)k^2} \sum_{j_{12} j_{12}' l l' J \varepsilon_I} (2J+1) |\delta_{v_1 j_1 v_2 j_2 l, v_1' j_1' v_2' j_2' l'} - S^{J \varepsilon_I}_{v_1 j_1 v_2 j_2 l, v_1' j_1' v_2' j_2' l'}(E)|^2, \quad (6)$$

where $(v_1 j_1 v_2 j_2)$ and $(v_1' j_1' v_2' j_2')$ are, respectively, the initial and final CMSs, the wave vector $k^2 = 2\mu E/\hbar^2$, and S is the scattering matrix. l is the orbital angular momentum and J the total collision system angular momentum, where $\vec{J} = \vec{l} + \vec{j}_{12}$ and $\vec{j}_{12} = \vec{j}_1 + \vec{j}_2$.

The total quenching cross section of CO from initial state $(v_1 j_1 v_2 j_2) \to (v_1'; v_2' j_2')$ was obtained by summing the state-to-state quenching cross sections over the final rotational state j_1' of CO in vibrational state v_1',

$$\sigma_{v_1 j_1 v_2 j_2 \to v_1'; v_2' j_2'}(E) = \sum_{j_1'} \sigma_{v_1 j_1 v_2 j_2 \to v_1' j_1' v_2' j_2'}(E). \quad (7)$$

Full-dimensional rovibrational scattering calculations were performed using the TwoBC code.[54] The CC equations were propagated for each value of R from 4 to 18.0 a_0 with step-size of $\Delta R = 0.05$ a_0 using the log-derivative matrix propagation method of Johnson[55] and Manolopoulos.[56] As discussed in Ref. 6, at least 13-15 rotational states have to be included in the $v_1 = 1$ basis set to ensure the convergence of the $v_1 = 1 \to 0$ vibrational quenching cross section. The cross sections are converged down to the lowest collision energy of 0.1 cm^{-1} based on tests with respect to the adopted maximum internuclear distance $R_{\max}$ for the long range part of the V6D PES. We further tested the effect of truncating $R_{\max}$ by performing pure rotational excitation and deexcitation calculations within the rigid-rotor approximation using the 4D V12 PES. No discernible difference was found for $R_{\max} = 18$ compared to $R_{\max} = 75$.

The number of discrete variable representation points N_{r_1} and N_{r_2}; the number of points in θ_1 and θ_2 for Gauss-Legendre quadrature, N_{θ_1} and N_{θ_2}; and the number of points in ϕ for Chebyshev quadrature, N_ϕ, adopted to project out the expansion coefficients of the interaction potential are listed in Table I. The intramolecular potentials used are $V_1(r_1)$ for the CO monomer presented by Huxley and Murrell[57] and $V_2(r_2)$ for the H_2 monomer adapted from the work of Schwenke.[58]

III. RESULTS AND DISCUSSION

A. Low energy pure rotational excitation

In Ref. 6, the pure rotational $j_1 = 0 \to 1$ excitation cross sections for $v_1 = 0$ of CO in collision with *para*-H_2 were calculated at low collision energies using the full-dimensional V6D and 4D V12 PESs. As indicated previously, the V12 PES[37] was calculated on a six-dimensional grid using high level electronic structure theory, then reduced to 4D by averaging over the ground intramolecular vibrations of CO and H_2. Results from the scattering calculations on the two PESs were convolved with an experimental energy spread function and compared to the measured relative cross sections of Chefdeville *et al.*[19] Except for the peak near 8 cm^{-1}, our calculation using V6D was in best agreement with the original experiment. More recently however, Chefdeville *et al.*[20] reported new measurements, new experimental analysis, and new calculations for the rotational excitation of CO with *normal*-H_2 and the rotational excitation from $j_1 = 0$ and 1 to $j_1' = 2$ of CO by *para*-H_2. The $j_1 = 0 \to 1$ measurement was re-analyzed following a procedure outlined in the work of Naulin and Costes[59] and theoretical cross sections were convolved using an adjusted experimental energy spread function. The $j_1 = 0 \to 1$ excitation cross sections shown in Fig. 3(a) of Ref. 6, which were obtained using the V6D and V12 PESs, are here convolved using the adjusted experimental energy spread. The new convolved theoretical cross sections

Reuse of AIP Publishing content is subject to the terms: https://publishing.aip.org/authors/rights-and-permissions. Downloaded to IP: 128.118.81.59 On: Wed, 23 Nov 2016 20:49:22

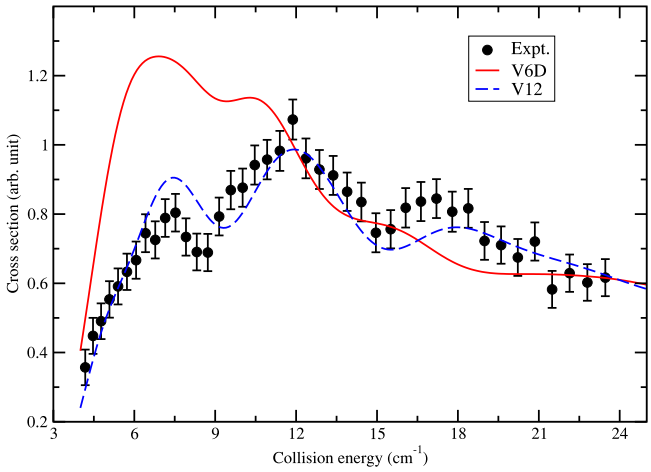

FIG. 4. $j_1 = 0 \rightarrow 1$ cross sections for CO($v_1 = 0$) due to collisions with $H_2(v_2 = 0, j_2 = 0)$ as a function of collision energy. The theoretical cross sections (lines) obtained using the V6D and 4D V12 PESs are convolved over the new experimental beam energy spread function to compare to the adjusted relative experiment of Chefdeville *et al.*[20] (circles with error bars).

are compared to the adjusted measurements in Fig. 4. In general, the cross section obtained with V12 shows good agreement with the new measurement. Though the V6D PES displayed better agreement with the original experiment as shown in Ref. 6, the new convolved cross sections obtained with V6D diverge from the adjusted measured data below ~12 cm^{-1}.

To compare with the additional measurements of Chefdeville *et al.*[20] for CO excitation ($j_1 = 0, 1 \rightarrow 2$) due to *para*-H_2 collisions and CO excitation ($j_1 = 0 \rightarrow 1$) by *normal* H_2, new full-dimensional and rigid-rotor approximation calculations of the state-to-state cross sections have been carried out using the V6D and V12 PESs, respectively. The MOLSCAT code[60] was used in the rigid-rotor calculations. The pure rotational excitation cross section calculated from the rigid-rotor calculations using a 4D PES, which was obtained by vibrationally averaging the V6D PES over ground vibrational states of CO and H_2, is nearly identical to the full-dimensional results, and therefore not shown. The computed cross sections were convolved with the new experimental energy function of Chefdeville *et al.*[20] In Fig. 5, $j_1 = 0, 1 \rightarrow 2$ cross sections for CO due to collisions with *para*-$H_2(j_2 = 0)$ are shown as a function of collision energy. Figs. 5(a) and 5(b) compare the computed cross sections for $j_1 = 0 \rightarrow 2$ and $j_1 = 1 \rightarrow 2$ transitions, respectively, using the V6D and V12 PESs. Fig. 5(c) shows the comparison between the total convolved theoretical cross sections and the relative experiment of Chefdeville *et al.*[20] Each total convolved theoretical cross section includes a 90% contribution from $j_1 = 0 \rightarrow 2$ and a 10% contribution from $j_1 = 1 \rightarrow 2$ transitions.

For the case of CO with *normal* H_2, the computed $j_1 = 0 \rightarrow 1$ rotational excitation cross sections of CO by *para*-H_2 ($j_2 = 0$) and *ortho*-H_2 ($j_2 = 1$) using the V6D and V12 PESs are compared in Figs. 6(a) and 6(b). The results of CO with *para*-H_2 are taken from Ref. 6. All the cross sections display strong resonances, particularly at collision energies below 18 cm^{-1}. Different resonance structures are exhibited

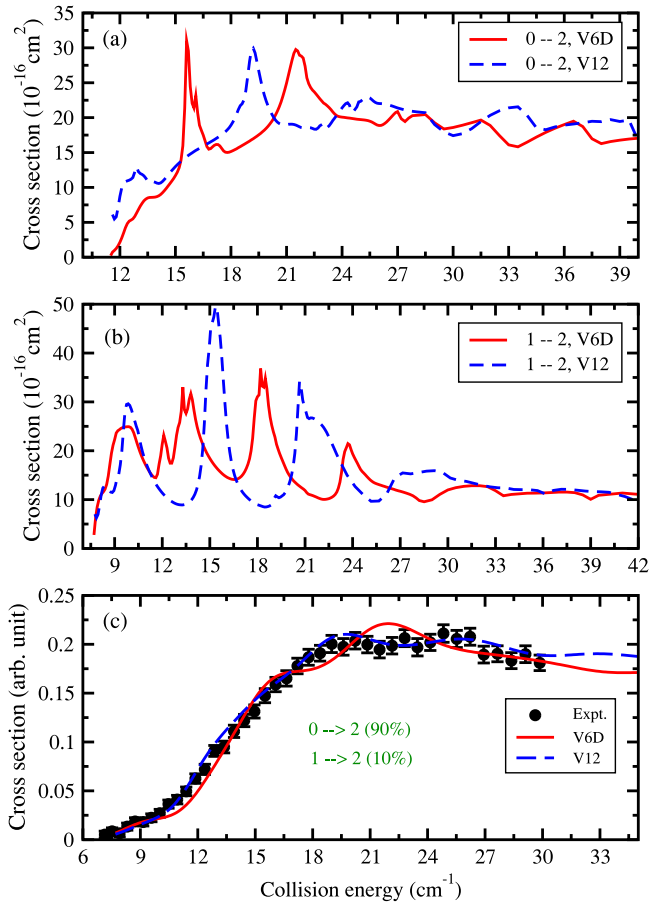

FIG. 5. $j_1 = 0, 1 \rightarrow 2$ cross sections for CO($v_1 = 0$) due to collisions with $H_2(v_2 = 0, j_2 = 0)$ as a function of collision energy. (a) $j_1 = 0 \rightarrow 2$ cross sections computed using the V6D and 4D V12 PESs. (b) $j_1 = 1 \rightarrow 2$ cross sections computed using the V6D and 4D V12 PESs. (c) Computed cross sections convolved over the new experimental beam energy spread function (lines) compared to the relative experiment of Chefdeville *et al.*[20] (circles with error bars).

for the V6D and V12 PESs. The convolved $j_1 = 0 \rightarrow 1$ cross section of CO by *normal* H_2 with 75% relative population of *ortho*-H_2 and 25% of *para*-H_2 is compared to the measurements in Fig. 6(c). It can be seen that the V12 PES shows good agreement with measurement over the whole experimental energy range. The V6D cross section is generally in good agreement with experiment, except near 9 cm^{-1}.

Overall, based on the comparison to adjusted experiments of Ref. 20, the low-energy pure rotational excitation cross sections from V12 PES show better agreement. The V6D PES appears to be less accurate for rotationally inelastic cross sections at low energies. Further improvements on the long-range part of the V6D PES may yield better agreement with experiment. As some uncertainty remains in the experimental analysis, perhaps, new measurements/improved analysis schemes would be useful. In particular, absolute cross sections would provide a more stringent discriminant. On the other hand, it is shown that the state-to-state cross sections on both PESs display numerous resonances and these resonances are very sensitive to the details of the PESs. The resonances generally shift by 2-3 cm^{-1} between V6D and V12 and this may be partially explained by the equilibrium geometries

Reuse of AIP Publishing content is subject to the terms: https://publishing.aip.org/authors/rights-and-permissions. Downloaded to IP: 128.118.81.59 On: Wed, 23 Nov 2016 20:49:22

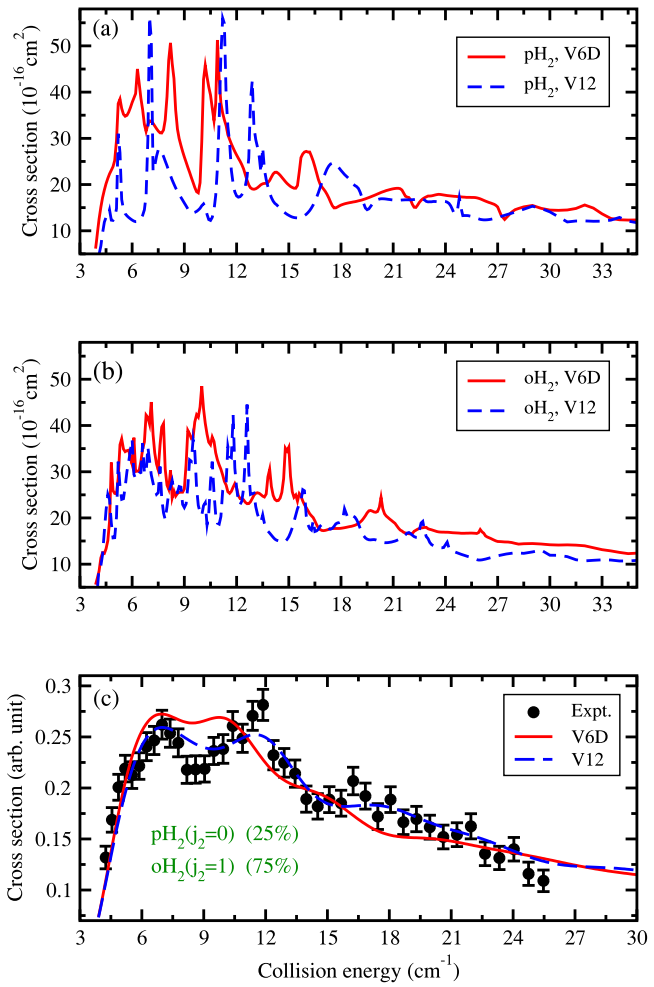

FIG. 6. $j_1 = 0 \rightarrow 1$ cross sections for CO($v_1 = 0$) due to collisions with *normal* $H_2(v_2 = 0)$ as a function of collision energy. (a) Computed cross sections due to collision with *para*-H_2 using the V6D and 4D V12 PESs. (b) Computed cross sections due to collision with *ortho*-H_2 using the V6D and 4D V12 PESs. (c) Computed cross sections convolved over the new experimental beam energy spread function (lines) compared to the relative experiment of Chefdeville *et al.*[20] (circles with error bars).

which for the vibrationally averaged surfaces have well depths of -83.82 cm^{-1} at $(R, \theta_1, \theta_2, \phi) = (7.926\ a_0, 180°, 0°, 0°)$ and -93.651 cm^{-1} at (7.911 a_0, 180°, 0°, 0°), respectively, for the V6D and V12 PESs. Furthermore, the differences in the well depths of the two PESs lead to differences in the energy level spectrum of the van der Waals complexes and corresponding resonance structures.

B. Rovibrational quenching

Full-dimensional calculations of the collision energy dependence of state-to-state cross sections were performed for initial CMSs $(1 j_1 0 j_2)$, for *para*-H_2 ($j_2 = 0$), and *ortho*-H_2 ($j_2 = 1$), $j_1 = 1$–5. The collision energy ranged from 0.1 to 1000 cm^{-1}. In this work, we consider only the rotation of H_2, and its vibration is fixed in the ground state $v_2 = v_2' = 0$.

Examples of the state-to-state cross sections for quenching from initial CMSs (1200) and (1401) into individual final CO rotational levels in $v_1 = 0$ are shown in Figs. 7 and 8, respectively, where $j_1' = 0, 2, 4, \ldots, 22$ and $j_2 = j_2'$ (i.e., elastic in H_2) are displayed. The insets show the distributions of final rotational levels of CO in $v_1' = 0$ at a collision energy of 2 cm^{-1}. As shown in Fig. 7, each of the cross sections decreases initially as the collision energy increases from 0.1 cm^{-1} exhibiting the threshold behavior predicted by Wigner's Law.[61] The cross sections display the presence of a number of resonances at energies between 1.0 and 30 cm^{-1}. The resonant relative magnitudes decrease with increasing of j_1'. Above the van der Waals region, the cross sections increase with increasing collision energy. Furthermore, the cross sections of larger j_1' increase faster. At a collision energy of 1000 cm^{-1}, the cross sections to $j_1' = 12$ and 22 merge and become the largest. An exception to this behavior is the CO rotational elastic transition to $j_1' = 2$, which has the largest cross section for collision energies below 20 cm^{-1} with less resonance like behavior between 1 and 30 cm^{-1}, and becomes the second smallest cross section at energies above 100 cm^{-1}. The inset of Fig. 7 shows CO final rotational distribution

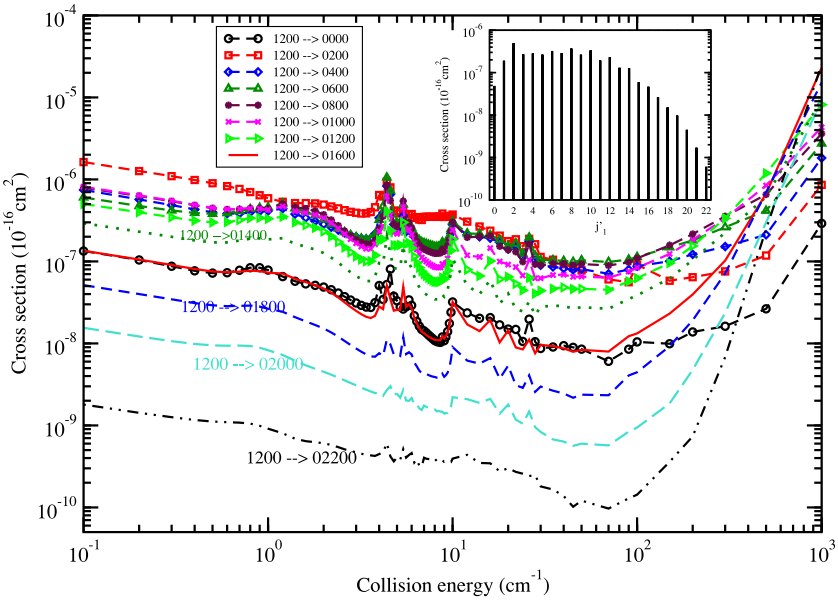

FIG. 7. State-to-state cross sections for vibrational quenching of CO from CMS (1200) to (0 j_1' 00). $j_1' = 0, 2, 4, \ldots, 22$ (odd j_1' are not shown for clarity). The inset shows the distributions of final rotational levels of CO in $v_1' = 0$ at collision energy of 2 cm^{-1}.

Reuse of AIP Publishing content is subject to the terms: https://publishing.aip.org/authors/rights-and-permissions. Downloaded to IP: 128.118.81.59 On: Wed, 23 Nov 2016 20:49:22

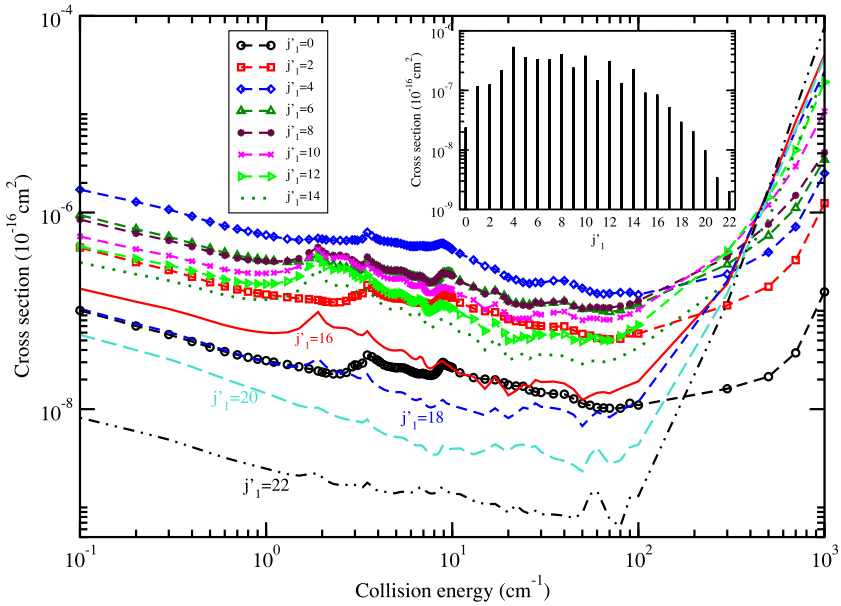

FIG. 8. State-to-state cross sections for vibrational quenching of CO from CMS (1401) to (0 j_1' 01). $j_1' = 0, 2, 4, \ldots, 22$. The inset shows the distributions of final rotational levels of CO in $v_1' = 0$ at the collision energy of 2 cm^{-1}.

in $v_1' = 0$ from quenching of (1200), and it can be seen that the final rotational distribution is broad and dominated by $\Delta j_1 = 0 - 10$. The distribution falls off rapidly above $j_1' = 16$.

For the vibrational quenching cross sections from CMS (1401) shown in Fig. 8, the trends noted for *para*-H_2 (1200) in Fig. 7 are also observed except for a suppression of resonance magnitudes. Similarly, for collision energies below 100 cm^{-1}, the CO rotational elastic transition dominates. At collision energies higher than 400 cm^{-1}, the cross section to $j_1' = 22$ gradually becomes the largest indicating that the rotational basis set may not be sufficient at high collision energies. The inset of Fig. 8 shows that the final rotational distribution of CO in $v_1' = 0$ from quenching of (1401) is broad and dominated by $\Delta j_1 = 0 - 10$ at a collision energy of 2 cm^{-1}.

In Fig. 9, the state-to-state quenching cross sections for CO from $v_1 = 1, j_1 = 3$ to $v_1' = 0, j_1'$ are compared between *para*-H_2 ($v_2 = 0, j_2 = 0$) and *ortho*-H_2 ($v_2 = 0, j_2 = 1$). The selected final rotational j_1' states are 1, 3, 7, 11, 15, and 19; H_2 rotational transitions are elastic. As shown in Fig. 9, for each individual transition, the state-to-state rovibrational quenching cross sections are of very similar shape and magnitude for the two colliders. The difference between *para*-H_2 and *ortho*-H_2 cross sections is somewhat larger at low collision energies, except for $j_1' = 19$ for which the cross sections are very similar. The inset presents the comparison of the distributions of final rotational levels j_1' in $v_1' = 0$ from quenching of (1300) and (1301) at a collision energy of 2.0 cm^{-1}. For these final j_1' levels, similar cross section magnitudes are observed for *para*-H_2 and *ortho*-H_2. Other final j_1' in $v_1' = 0$ which are not shown in Fig. 9 result in similar cross section trends.

Using Eq. (7), the state-to-state cross sections from each initial CMS are summed over all final rotational states j_1' in v_1' to obtain the total vibrational quenching cross sections as a function of collision energy. Figs. 10-12 depict the total quenching cross sections of CO from CMSs ($1j_10j_2$), $j_1 = 1$, 3, and 5 with $j_2 = 0$. As shown in Table I, the basis sets

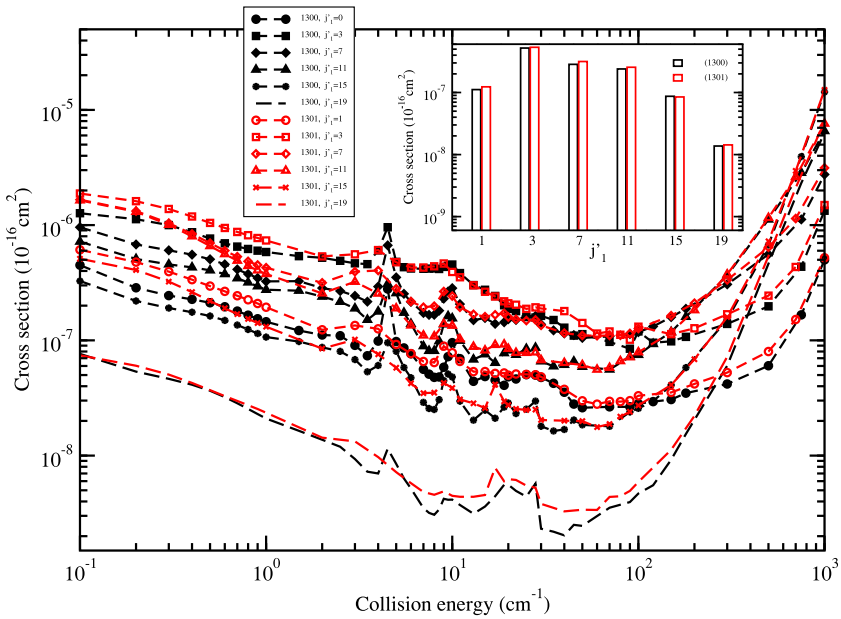

FIG. 9. Comparison of the state-to-state cross sections for vibrational quenching of CO in collisions with *para*-H_2 from CMS (1300) and with *ortho*-H_2 from CMS (1301), and H_2 rotational transitions are elastic. The final rotational j_1' states shown are 1, 3, 7, 11, 15, and 19. The inset compares the distributions of final rotational levels of CO in $v_1' = 0$ at collision energy of 2 cm^{-1} between *para*-H_2 and *ortho*-H_2.

Reuse of AIP Publishing content is subject to the terms: https://publishing.aip.org/authors/rights-and-permissions. Downloaded to IP: 128.118.81.59 On: Wed, 23 Nov 2016 20:49:22

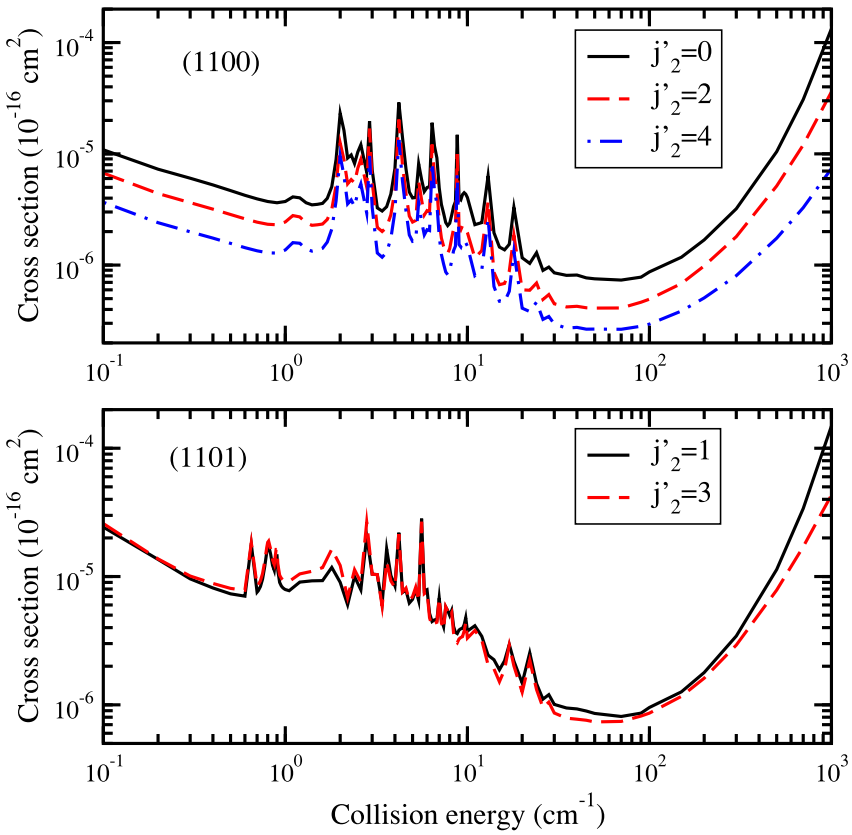

FIG. 10. Total cross sections for vibrational quenching of CO from $(v_1 = 1, j_1 = 1;\ v_2 = 0, j_2)$ to $(v_1' = 0; v_2' = 0, j_2')$. Upper panel: CO with *para*-H_2, $j_2 = 0$, $j_2' = 0$, 2, and 4. Lower panel: CO with *ortho*-H_2, $j_2 = 1$, $j_2' = 1$ and 3.

include rotational states 0, 2, and 4 for *para*-H_2 and 1 and 3 for *ortho*-H_2. For all initial CO j_1 states, the upper panels show the CO total quenching cross sections for H_2 rotational transitions $j_2 = 0 \rightarrow j_2' = 0$, 2, and 4, and the lower panels show the CO total quenching cross sections for H_2 rotational transitions $j_2 = 1 \rightarrow j_2' = 1$ and 3. Figs. 10-12 show clearly that the cross sections exhibit almost the same trends for each initial CO j_1 state. The total quenching cross sections show

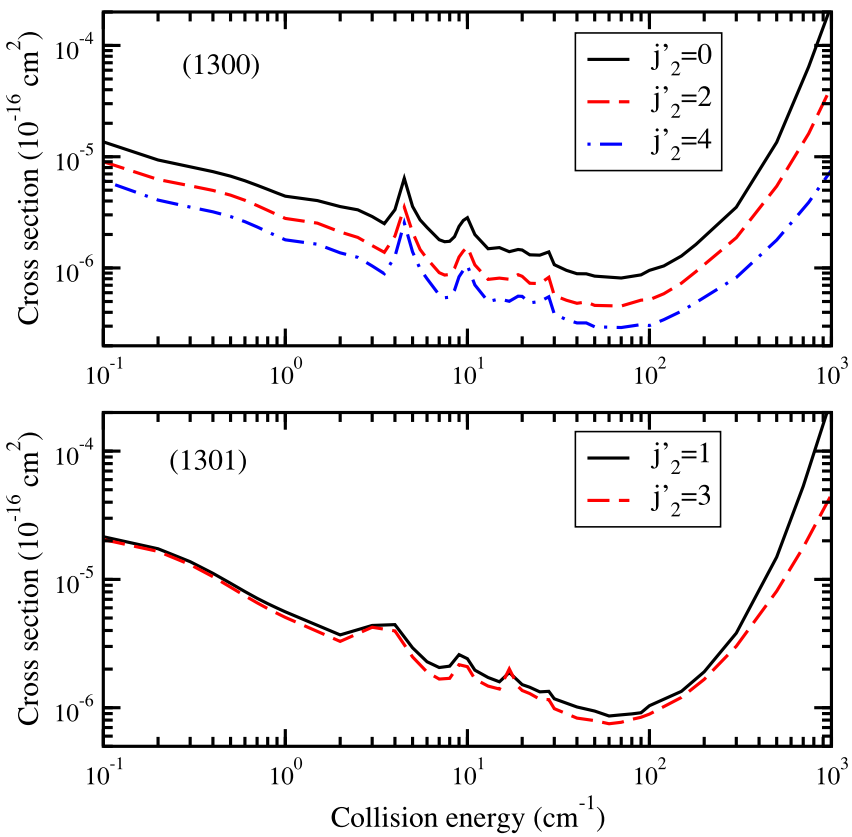

FIG. 11. Same as Fig. 10, except for $j_1 = 3$.

Reuse of AIP Publishing content is subject to the terms: https://publishing.aip.org/authors/rights-and-permissions. Downloaded to IP: 128.118.81.59 On: Wed, 23 Nov 2016 20:49:22

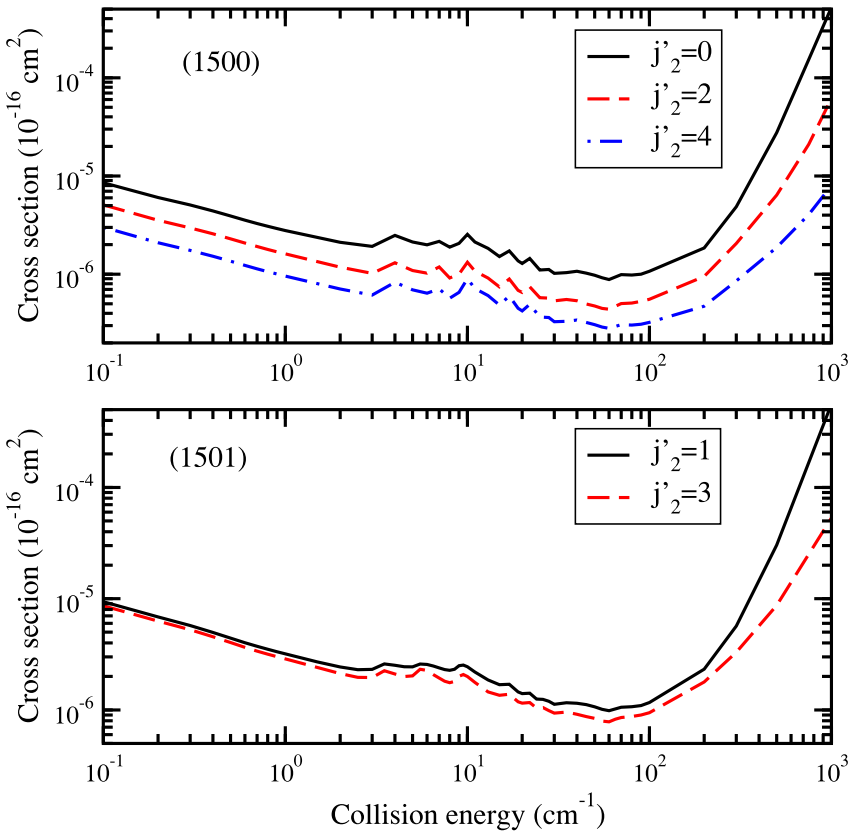

FIG. 12. Same as Fig. 10, except for $j_1 = 5$.

qualitatively similar structure with a number of resonances in the energy range between 0.7 and 30 cm^{-1} induced by the van der Waals interaction, like those shown in Figs. 7 and 8 for the state-to-state cross sections. However the suppression of the resonances can be found with increasing initial CO rotational quantum number j_1. While for energies higher than 70 cm^{-1} the cross sections increase with increasing collision energy. Further observation shows that for CO with *para*-H_2, over the whole collision energy range elastic H_2 transitions are dominant over inelastic H_2 transitions with $\Delta j_2 = 4$ being the smallest. While for the case of *ortho*-H_2 below 100 cm^{-1}, the cross sections for elastic and inelastic H_2 transitions are of similar magnitude. We note that this may be an artifact of the small *ortho*-H_2 basis, but we are currently limited by memory considerations. For collision energies greater than 100 cm^{-1}, the cross section difference between elastic and inelastic H_2 transitions increases with increasing collision energy.

In Fig. 13, the total cross sections for vibrational quenching of CO with *para*-H_2 from $(1j_100)$ to $(v_1' = 0; v_2' = 0, j_2' = 0)$ are compared for $j_1 = 0$–5. The result for $j_1 = 0$, taken from Ref. 6, shows the strongest resonances at relatively low collision energies. The resonances decrease

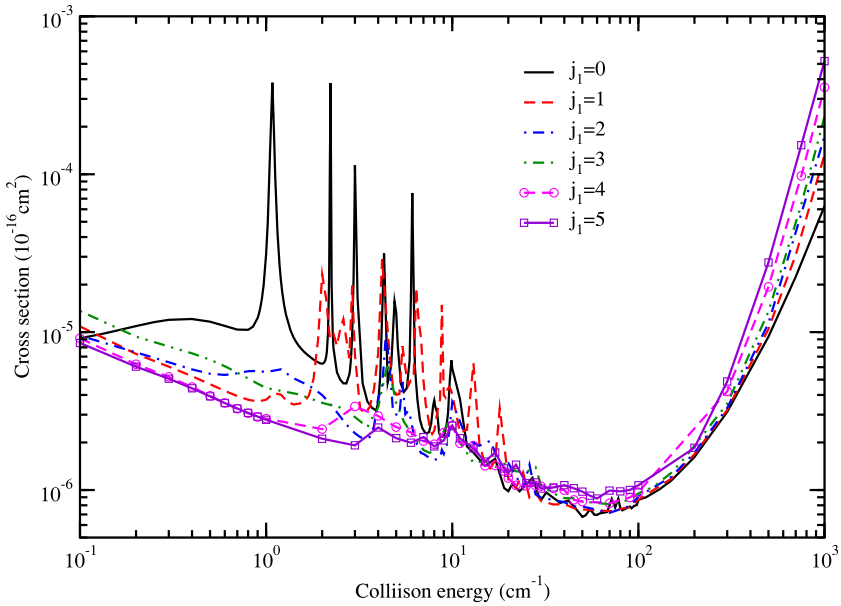

FIG. 13. Comparison of the total cross sections for vibrational quenching of CO with *para*-H_2 from $(1j_100)$ to $(v_1' = 0; v_2' = 0, j_2' = 0)$, $j_1 = 0$, 1, 2, 3, 4, and 5.

Reuse of AIP Publishing content is subject to the terms: https://publishing.aip.org/authors/rights-and-permissions. Downloaded to IP: 128.118.81.59 On: Wed, 23 Nov 2016 20:49:22

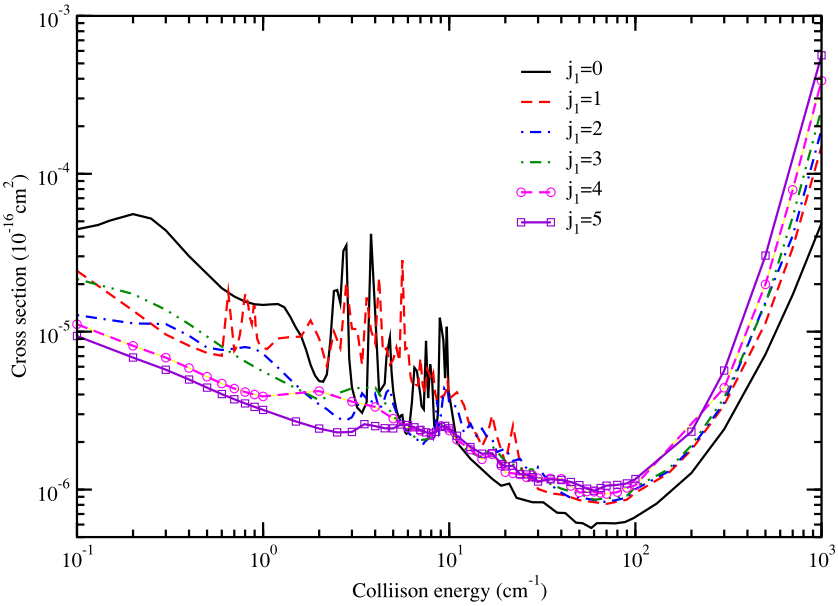

FIG. 14. Comparison of the total cross sections for vibrational quenching of CO with *ortho*-H_2 from $(1j_101) \rightarrow (v_1'=0; v_2'=0, j_2'=1)$, $j_1=0$, 1, 2, 3, 4, and 5.

with increasing j_1, with the total cross section of $j_1 = 5$ having the weakest resonances. As the collision energy increases, the cross section for $j_1 = 5$ becomes the largest with $j_1 = 0$ being the smallest. The total cross sections for vibrational quenching of CO with *ortho*-H_2 from $(1j_101)$ to $(v_1' = 0; v_2' = 0, j_2' = 1)$ for $j_1 = 0$–5 are displayed in Fig. 14. The comparison shows similar behavior as found for *para*-H_2 in Fig. 13, except that the resonances are more suppressed.

For each CO initial rotational quantum number $j_1 = 0$–5 in the $v_1 = 1$ state, Fig. 15 presents comparisons of the total cross sections of vibrational quenching of CO with *para*-H_2 and *ortho*-H_2 from $(1j_10j_2) \rightarrow (v_1' = 0; v_2' = 0, j_2')$ and H_2 rotational transitions remaining elastic. As shown in Fig. 15, there are small differences between *para*-H_2 and *ortho*-H_2 for low collision energies, with the differences becoming smaller with increasing j_1. For collision energies above 10 cm^{-1}, the cross sections of the two colliders are very similar. In Fig. 15(a), the total cross sections of Flower[34] for the vibrational de-excitation of CO($v_1 = 1$) by *para*-H_2 and by *ortho*-H_2 are also presented. The CC method was adopted in Flower's calculations, but with a 4D PES. There is a two order of magnitude dispersion between the current results and Flower's. As discussed in Ref. 6, this is due to the difference between 6D and 4D PESs and the fact that Flower likely used an insufficient CO basis in the scattering calculations.

In addition to rovibrational quenching calculations from CO $v_1 = 1$, we also carried out quenching calculations from the CO $v_1 = 2$ state, with CMS (2000). The total cross sections

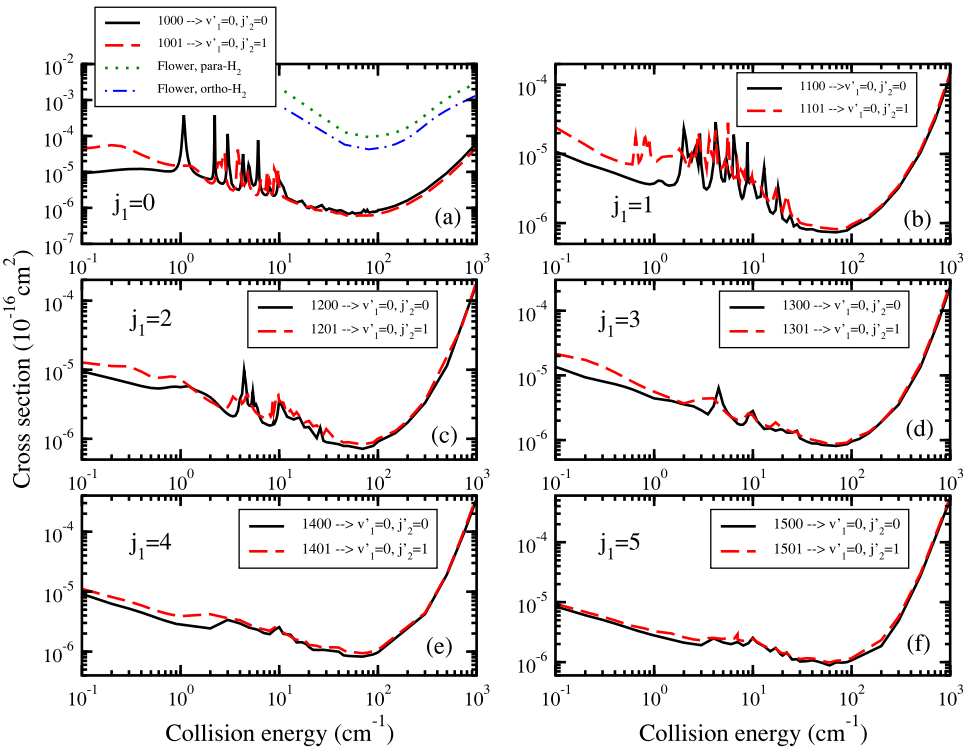

FIG. 15. Comparison of the total cross sections of vibrational quenching of CO in collision with *para*- and *ortho*-H_2 from $(1j_10j_2) \rightarrow (v_1' = 0; v_2' = 0, j_2')$. *para*-$H_2$: $j_2 = j_2' = 0$, *ortho*-H_2: $j_2 = j_2' = 1$. (a) $j_1 = 0$, (b) $j_1 = 1$, (c) $j_1 = 2$, (d) $j_1 = 3$, (e) $j_1 = 4$, (f) $j_1 = 5$. In (a) the total cross sections of Flower[34] for the vibrational de-excitation of CO($v_1 = 1, j_1 = 0$) by *para*-H_2 and by *ortho*-H_2 are also presented.

Reuse of AIP Publishing content is subject to the terms: https://publishing.aip.org/authors/rights-and-permissions. Downloaded to IP: 128.118.81.59 On: Wed, 23 Nov 2016 20:49:22

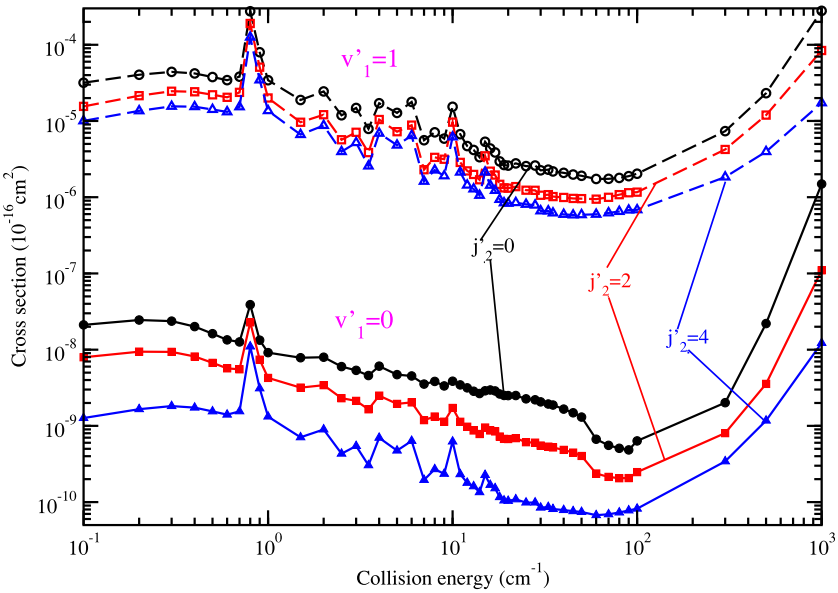

FIG. 16. Total cross sections for vibrational quenching of CO with $para$-H_2 for $(2000) \rightarrow (v_1'; v_2' = 0, j_2')$ with $v_1' = 0$ and 1; $j_2' = 0$, 2, and 4.

of CO for vibrational quenching $v_1 = 2 \rightarrow v_1' = 1$ and $v_1 = 2 \rightarrow v_1' = 0$ are presented in Fig. 16. For each $\Delta v_1 = v_1' - v_1$ quenching, H_2 rotational transitions are $j_2 \rightarrow j_2' = 0$, 2, and 4. As can be seen in Fig. 16, the total quenching cross sections for both $\Delta v_1 = -1$ and -2 show similar behavior, display resonances at low collision energies, reach minima near 50 cm^{-1}, and then increase with increasing collision energy. The cross sections with H_2 rotationally elastic are the largest. It can also be seen from this figure that the cross section of $\Delta v_1 = -1$ quenching is about two to three orders of magnitude larger than those of $\Delta v_1 = -2$ quenching. This indicates that for a high initial vibrational state, the $\Delta v_1 = -1$ transition dominates the vibrational quenching process as expected due to the highly harmonic character of the CO potential energy. In Fig. 17 the total cross sections of CO quenching from $v_1 = 2 \rightarrow v_1' = 1$ are compared with the results of CO vibrational quenching $v_1 = 1 \rightarrow v_1' = 0$, the initial CMSs are (2000) and (1000), and H_2 final rotational states are $j_2' = 0$ and 2. As can be seen the cross sections for quenching $v_1 = 1 \rightarrow v_1' = 0$ show significant resonance structure with some sharp features at certain collision energies. In contrast to the quenching of $v_1 = 1 \rightarrow v_1' = 0$, the cross sections for quenching $v_1 = 2 \rightarrow v_1' = 1$ show different resonance structure with less sharp features. However, the magnitude of the cross sections is observed to be approximately three times larger than those of $v_1 = 1 \rightarrow v_1' = 0$.

Additionally, we computed the CO pure rotational quenching cross sections within the vibrational state $v_1 = 0$ and 1. In each vibrational state, rotational quenching was performed for initial CO rotational states $j_1 = 1$–5 with the H_2 rotational transition elastic ($para$-H_2, $j_2 = 0$ and $ortho$-H_2, $j_2 = 1$). As examples, Fig. 18 shows the pure rotational quenching in CO $v_1 = 1$. Cross sections are from $j_1 = 1$, 3, and 5 to all possible lower levels for CO in collisions with $para$-H_2 and $ortho$-H_2, respectively. In contrast to the vibrational quenching cross sections, the pure rotational cross sections are significantly larger. In the case of CO with $para$-H_2, the quenching cross sections of $j_1 = 3$ are dominated by the

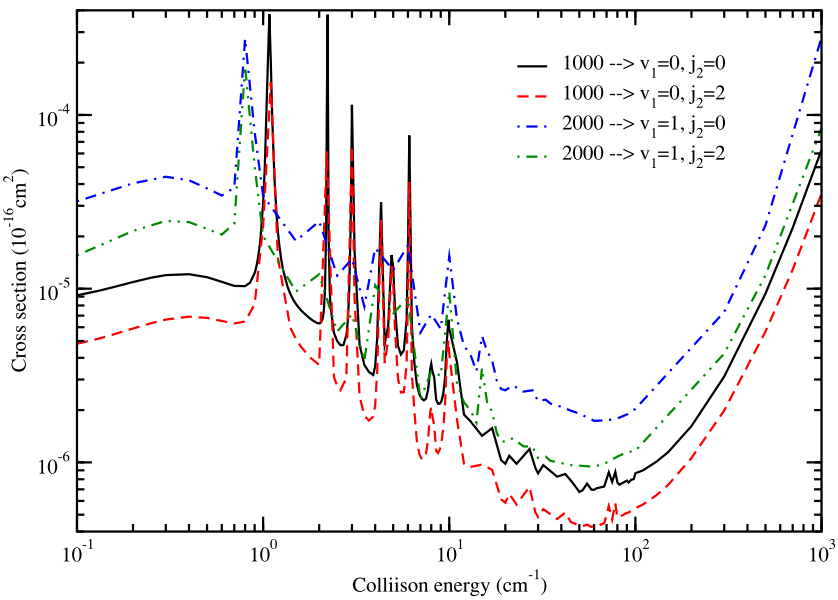

FIG. 17. Comparison of the total cross sections of $\Delta v_1 = -1$ vibrational quenching of CO in collision with $para$-H_2 from CMSs (2000) and (1000). H_2 final rotational states are $j_2' = 0$ and 2.

Reuse of AIP Publishing content is subject to the terms: https://publishing.aip.org/authors/rights-and-permissions. Downloaded to IP: 128.118.81.59 On: Wed, 23 Nov 2016 20:49:22

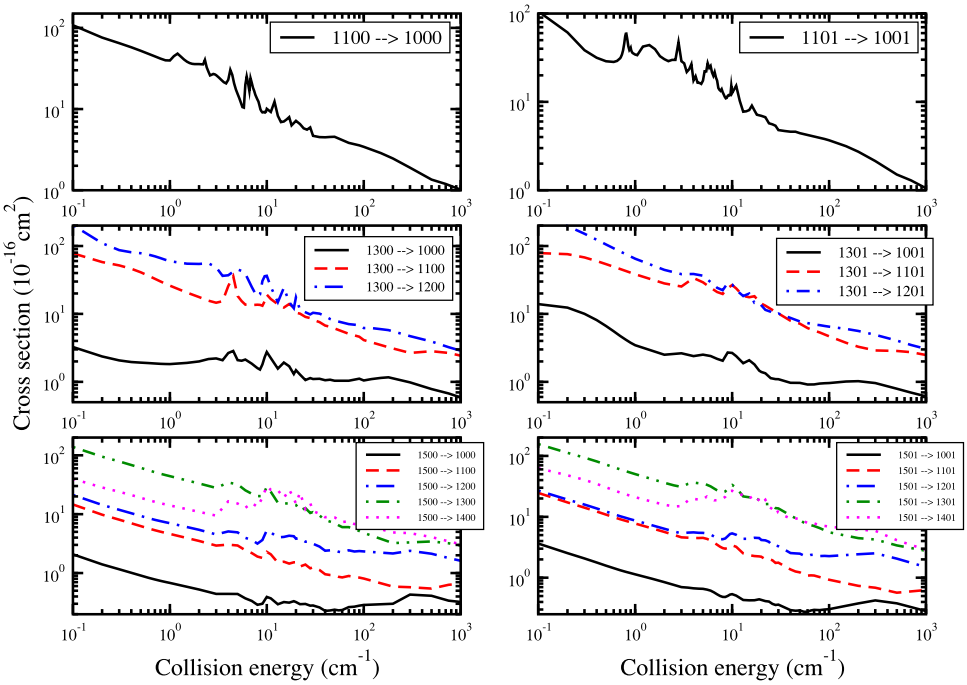

FIG. 18. Pure rotational cross sections for $(1j_10j_2) \rightarrow (1j_1'0j_2)$ transitions. $j_1 = 1$, 3, and 5, $j_1' < j_1$. Left panels: CO with *para*-H_2, $j_2 = 0$; right panels: CO with *ortho*-H_2, $j_2 = 1$.

$3 \rightarrow 2$ transition, the smallest cross section is for $j_1 = 3 \rightarrow 0$ transition. For initial $j_1 = 5$, the smallest cross section is still for final $j_1' = 0$; however, the dominant transition varies with collision energy. When the collision energy is below 10 cm^{-1}, the cross section for the $j_1 = 5 \rightarrow 3$ transition is the largest. Above 10 cm^{-1}, the transition $j_1 = 5 \rightarrow 4$ dominates. In the case of pure rotational quenching of CO by *ortho*-H_2, the trends found for *para*-H_2 are also evident as displayed in Fig. 18. Given a CO rotational quenching $j_1 \rightarrow j_1'$, the ratios of the cross sections of CO in collisions with *para*-H_2 to the cross sections of *ortho*-H_2 are presented in Fig. 19. The initial CO rotational state is $j_1 = 1$, 3, and 5. It can be seen from

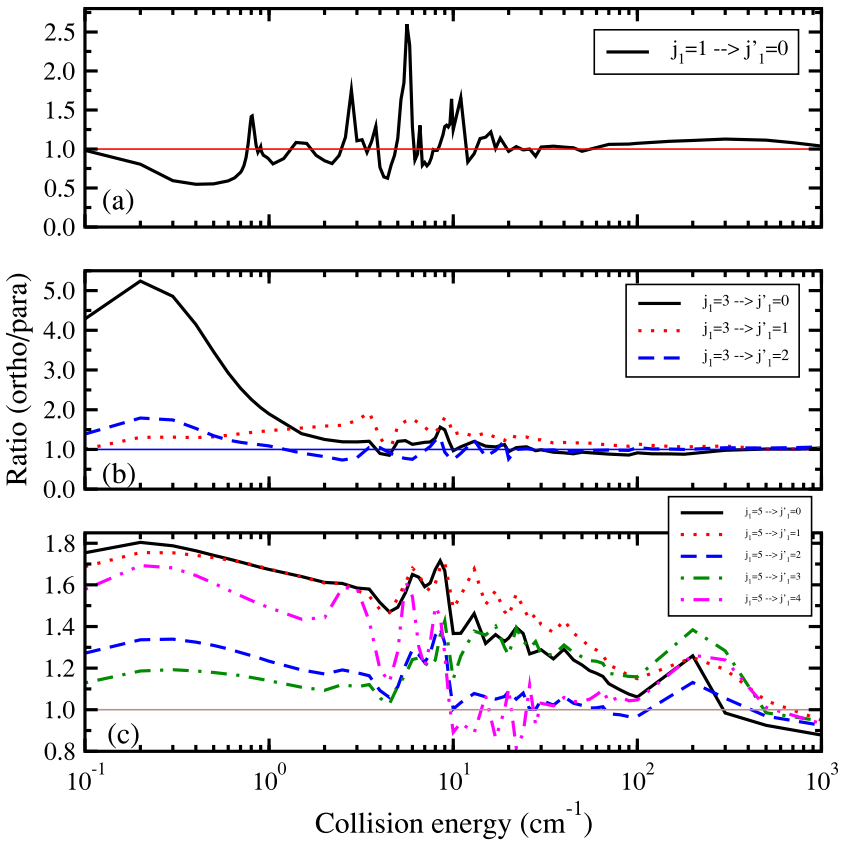

FIG. 19. Ratios of the cross sections of CO with *para*-H_2 to those of CO with *ortho*-H_2 for rotational transitions $(1j_10j_2)$ to $(1j_1'0j_2')$, for *para*-H_2 $(j_2 = j_2' = 0)$, *ortho*-H_2 $(j_2 = j_2' = 1)$. (a) $j_1 = 1$, (b) $j_1 = 3$, (c) $j_1 = 5$.

Reuse of AIP Publishing content is subject to the terms: https://publishing.aip.org/authors/rights-and-permissions. Downloaded to IP: 128.118.81.59 On: Wed, 23 Nov 2016 20:49:22

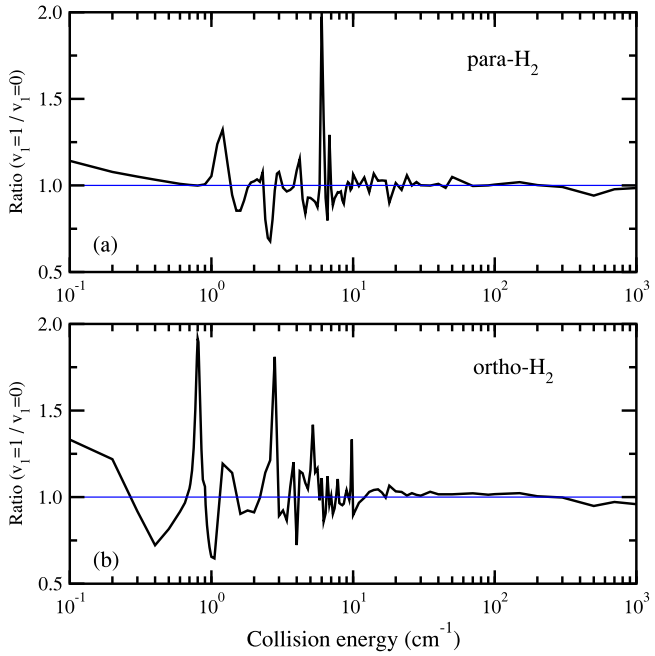

FIG. 20. Ratios of the pure rotational $j_1 = 1 \rightarrow j_1' = 0$ quenching cross sections of CO in $v_1 = 1$ to those of CO in $v_1 = 0$. (a) CO with $para$-H_2, rotational transitions are (0100) → (0000) and (1100) → (1000); (b) CO with $ortho$-H_2, rotational transitions are (0101) → (0001) and (1101) → (1001).

the figure that rotational state-to-state cross sections show differences at low collision energies, where the ratios show large fluctuations due to resonances. Starting from roughly 10 cm^{-1}, the cross sections of $para$-H_2 and $ortho$-H_2 are of similar magnitude with ratios typically $\lesssim$1.5.

For CO pure rotational quenching cross section from $j_1 = 1$ to $j_1' = 0$ in $v_1 = 0$ and 1, we consider here the transitions (0100) → (0000) and (1100) → (1000) for $para$-H_2 and (0101) → (0001) and (1101) → (1001) for $ortho$-H_2. In Fig. 20 the ratios of cross sections within $v_1 = 1$ to those within $v_1 = 0$ are displayed for $para$-H_2 and $ortho$-H_2, respectively. Despite some differences at low collision energy, where the ratios show large fluctuations in the resonance regions, the $j_1 = 1 \rightarrow j_1' = 0$ cross sections in $v_1 = 1$ are almost the same as those for $v_1 = 0$. In other words, the CO rotational state-to-state cross section in excited vibrational levels can be approximately estimated from the results in $v_1 = 0$ for collision energies above 10 cm^{-1}, which is likely related to the harmonic nature of the CO potential.

IV. ASTROPHYSICAL APPLICATION

Molecular hydrogen and carbon monoxide are the most abundant molecular species in the majority of interstellar environments. CO has a large dissociation energy and is stable at low temperatures; therefore, it is widespread and a good tracer of molecular gas.[62] Most studies have focused on pure rotational transitions observed in the far infrared to the radio or electronic absorption in the near ultraviolet. Recently pure rotational transitions in the CO vibrational states $v_1 = 1$ and 2 were detected in the circumstellar shell of the star IRC +10 216.[63] In particular, CO vibrational transitions have been detected; for example, emission due to the fundamental vibrational band near 4.7 μm was observed in star-forming regions in Orion with the *Infrared Space Observatory*[64] and from protoplanetary disks (PPDs) of young stellar objects[65–67] with the Gemini Observatory and the Very Large Telescope (VLT). Our current full-dimensional scattering calculation is able to provide accurate rovibrational state-to-state CO–H_2 collisional data for future modeling of protostars, the infrared sources discussed above, and future FIR and submillimeter observations with *Herschel* and the VLT. Further, CO vibrational bands in the 1-5 μm region will be accessible by the *James Webb Space Telescope* to be launched in 2018. In PPDs, CO vibrational lines probe the inner warm regions which are exposed to the UV radiation from the protostar.

V. SUMMARY

Full-dimensional dynamics computations for inelastic rovibrational quenching of CO due to H_2 impact have been carried out for initial combined molecular states ($1j_10j_2$), j_1 = 1-5, and (2000) with $j_2 = 0$ and 1 for $para$-H_2 and $ortho$-H_2, respectively. The full-dimensional scattering calculations were performed on a 6D CO–H_2 interaction potential surface computed with high-level electronic structure theory and fitted with an invariant polynomial approach. See the supplementary material for a FORTRAN code to compute the V6D PES.[68] In addition, pure rotational excitation of CO ($v_1 = 0$) in collision with $para$-, $ortho$-, and $normal$-H_2 was computed. All scattering calculations were done within a full angular-momentum-coupling formulation and compared to available experimental data and prior calculations. In general, good agreement was found between full-dimensional calculations and available measurements, as highlighted in Ref. 6, but additional inelastic experiments which obtain absolute cross sections, particularly for cold collision energies, would be desirable. Both state-to-state and total quenching cross sections from CO vibrational states $v_1 = 1$ and $v_1 = 2$ show resonance structures at intermediate energies. The V12 PES appears to be more accurate for pure rotationally inelastic collisions at low energies, while the present V6D PES is appropriate for vibrationally inelastic collisions. To further improve V6D, it will be extended to long-range in the future, but in six-dimensions. The current calculations together with large scale coupled-states (CS) approximation[8] results will be essential in the construction of a database of CO rovibrational quenching rate coefficients urgently needed for astrophysical modeling including that of the inner zone of protoplanetary disks.

ACKNOWLEDGMENTS

The work at UGA and Emory was supported by NASA Grant No. NNX12AF42G from the Astronomy and Physics Research and Analysis Program, at UNLV by NSF Grant No. PHY-1505557, and at Penn State by NSF Grant No. PHY-1503615. This study was supported in part by resources and technical expertise from the UGA Georgia Advanced

Reuse of AIP Publishing content is subject to the terms: https://publishing.aip.org/authors/rights-and-permissions. Downloaded to IP: 128.118.81.59 On: Wed, 23 Nov 2016 20:49:22

Computing Resource Center (GACRC), a partnership between the UGA Office of the Vice President for Research and Office of the Vice President for Information Technology. We thank Shan-Ho Tsai (GACRC), Jeff Deroshia (UGA Department of Physics and Astronomy), and Greg Derda (GACRC) for computational assistance. We thank A. Bergeat for providing us with their experimental data.

[1]S. K. Pogrebnya and D. C. Clary, Chem. Phys. Lett. **363**, 523 (2002).
[2]A. N. Panda, F. Otto, F. Gatti, and H.-D. Meyer, J. Chem. Phys. **127**, 114310 (2007).
[3]G. Quéméner and N. Balakrishnan, J. Chem. Phys. **130**, 114303 (2009).
[4]S. F. dos Santos, N. Balakrishnan, S. Lepp, G. Quéméner, R. C. Forrey, R. J. Hinde, and P. C. Stancil, J. Chem. Phys. **134**, 214303 (2011).
[5]S. F. dos Santos, N. Balakrishnan, R. C. Forrey, and P. C. Stancil, J. Chem. Phys. **138**, 104302 (2013).
[6]B. H. Yang, P. Zhang, X. Wang, P. C. Stancil, J. M. Bowman, N. Balakrishnan, and R. C. Forrey, Nat. Commun. **6**, 6629 (2015).
[7]A. Bohr, S. Paolini, R. C. Forrey, N. Balakrishnan, and P. C. Stancil, J. Chem. Phys. **140**, 064308 (2014).
[8]R. C. Forrey, B. H. Yang, P. C. Stancil, and N. Balakrishnan, Chem. Phys. **462**, 71 (2015).
[9]A. J. Andrews and C. J. S. M. Simpson, Chem. Phys. Lett. **36**, 271 (1975).
[10]A. J. Andrews and C. J. S. M. Simpson, Chem. Phys. Lett. **41**, 565 (1976).
[11]G. J. Wilson, M. L. Turnidge, A. S. Solodukhin, and C. J. S. M. Simpson, Chem. Phys. Lett. **207**, 521 (1993).
[12]A. Kudian, H. L. Welsh, and A. Watanabe, J. Chem. Phys. **47**, 1553 (1967).
[13]P. Andresen, H. Joswig, H. Pauly, and R. Schinke, J. Chem. Phys. **77**, 2204 (1982).
[14]A. Picard-Bersellini, R. Charneau, and P. Brechignac, J. Chem. Phys. **78**, 5900 (1983).
[15]B. Schramm, E. Elias, L. Kern, G. Natour, A. Schmitt, and C. Weber, Ber. Bunsenges. Phys. Chem. **95**, 615 (1991).
[16]T. Drascher, T. F. Giesen, T. Y. Yang, N. Schmucker, R. Schieder, G. Winnewisser, P. Joubert, and J. Bonamy, J. Mol. Spectrosc. **192**, 268 (1998).
[17]A. R. W. McKellar, J. Chem. Phys. **108**, 1811 (1998).
[18]S. Antonova, A. P. Tsakotellis, A. Lin, and G. C. McBane, J. Chem. Phys. **112**, 554 (2000).
[19]S. Chefdeville, T. Stoecklin, A. Bergeat, K. M. Hickson, C. Naulin, and M. Costes, Phys. Rev. Lett. **109**, 023201 (2012).
[20]S. Chefdeville, T. Stoecklin, C. Naulin, P. Jankowski, K. Szalewicz, A. Faure, M. Costes, and A. Bergeat, Astrophys. J. Lett. **799**, L9 (2015).
[21]S. Green and P. Thaddeus, Astrophys. J. **205**, 766 (1976).
[22]D. R. Flower, J. M. Launay, E. Kochanski, and J. Prissette, Chem. Phys. **37**, 355 (1979).
[23]L. L. Poulsen, Chem. Phys. **68**, 29 (1982).
[24]R. Schinke, H. Meyer, U. Buck, and G. H. F. Diercksen, J. Chem. Phys. **80**, 5518 (1984).
[25]Z. Bačić, R. Schinke, and G. H. F. Diercksen, J. Chem. Phys. **82**, 236 (1985).
[26]Z. Bačić, R. Schinke, and G. H. F. Diercksen, J. Chem. Phys. **82**, 245 (1985).
[27]C. A. Parish, J. D. Augspurger, and C. E. Dykstra, J. Phys. Chem. **96**, 2069 (1992).
[28]G. Danby, J. Furlong, D. Lodge, S. Miller, and A. Patel, J. Phys. B **26**, 4127 (1993).
[29]M. C. Salazar, A. de Castro, J. L. Paz, G. H. F. Diercksen, and A. J. Hernandez, Int. J. Quantum Chem. **55**, 251 (1995).
[30]J. P. Reid, C. J. S. M. Simpson, and H. M. Quiney, J. Chem. Phys. **106**, 4931 (1997).
[31]M. Mengel, F. C. DeLucia, and E. Herbst, Can. J. Phys. **79**, 589 (2001).
[32]R. Kobayashi, R. D. Amos, J. P. Reid, H. M. Quiney, and C. J. S. M. Simpson, Mol. Phys. **98**, 1995 (2000).
[33]D. R. Flower, J. Phys. B **34**, 2731 (2001).
[34]D. R. Flower, Mon. Not. R. Astron. Soc. **425**, 1350 (2012).
[35]P. Jankowski and K. Szalewicz, J. Chem. Phys. **108**, 3554 (1998).
[36]P. Jankowski and K. Szalewicz, J. Chem. Phys. **123**, 104301 (2005).
[37]P. Jankowski, L. A. Surin, A. Potapov, S. Schlemmer, A. R. W. McKellar, and K. Szalewicz, J. Chem. Phys. **138**, 084307 (2013).
[38]H. Li, X.-L. Zhang, R. J. Le Roy, and P.-N. Roy, J. Chem. Phys. **139**, 164315 (2013).
[39]M. Wernli, P. Valiron, A. Faure, L. Wiesenfeld, P. Jankowski, and K. Szalewicz, Astron. Astrophys. **446**, 367 (2006).
[40]B. H. Yang, P. C. Stancil, N. Balakrishnan, and R. C. Forrey, J. Chem. Phys. **124**, 104304 (2006); Erratum **125**, 079904 (2006).
[41]B. H. Yang, P. C. Stancil, N. Balakrishnan, and R. C. Forrey, Astrophys. J. **718**, 1062 (2010).
[42]B. J. Braams and J. M. Bowman, Int. Rev. Phys. Chem. **28**, 577 (2009).
[43]H.-J. Werner, P. J. Knowles, G. Knizia, F. R. Manby, M. Schütz *et al.*, MOLPRO, version 2010.1, a package of *ab initio* programs, 2010, see http://www.molpro.net.
[44]T. B. Adler, G. Knizia, and H.-J. Werner, J. Chem. Phys. **127**, 221106 (2007).
[45]H.-J. Werner, T. B. Adler, and F. R. Manby, J. Chem. Phys. **126**, 164102 (2007).
[46]J. G. Hill, S. Mazumder, and K. A. Peterson, J. Chem. Phys. **132**, 054108 (2010).
[47]F. Bernardi and S. F. Boys, Mol. Phys. **19**, 553 (1970).
[48]D. Feller, K. A. Peterson, and J. G. Hill, J. Chem. Phys. **133**, 184102 (2010).
[49]A. Arthurs and A. Dalgarno, Proc. R. Soc. London, Ser. A **256**, 540 (1960).
[50]K. Takayanagi, Adv. At. Mol. Phys. **1**, 149 (1965).
[51]S. Green, J. Chem. Phys. **62**, 2271 (1975).
[52]M. H. Alexander and A. E. DePristo, J. Chem. Phys. **66**, 2166 (1977).
[53]G. Zarur and H. Rabitz, J. Chem. Phys. **60**, 2057 (1974).
[54]R. V. Krems, *TwoBC–Quantum Scattering Program* (University of British Columbia, Vancouver, Canada, 2006).
[55]B. R. Johnson, J. Comput. Phys. **13**, 445 (1973).
[56]D. E. Manolopoulos, J. Chem. Phys. **85**, 6425 (1986).
[57]P. Huxley and J. N. Murrell, J. Chem. Soc., Faraday Trans. 2 **79**, 323 (1983).
[58]D. W. Schwenke, J. Chem. Phys. **89**, 2076 (1988).
[59]C. Naulin and M. Costes, Int. Rev. Phys. Chem. **33**, 427 (2014).
[60]J. M. Hutson and S. Green, MOLSCAT computer code (distributed by Collaborative Computational Project No. 6 of the United Kingdom Engineering and Physical Sciences Research Council, Swindon, 1994), Version 14.
[61]E. P. Wigner, Phys. Rev. **73**, 1002 (1948).
[62]N. Neininger, M. Guelin, H. Ungerechts, R. Lucas, and R. Wielebinski, Nature **395**, 871 (1998).
[63]N. A. Patel, K. H. Young, S. Brünken, K. M. Menten, P. Thaddeus, and R. W. Wilson, Astrophys. J. **691**, L55 (2009).
[64]E. González, C. M. Wright, J. Cernicharo, D. Rosenthal, A. M. S. Boonman, and E. F. van Dishoeck, Astron. Astrophys. **386**, 1074 (2002).
[65]S. D. Brittain, J. R. Najita, and J. S. Carr, Astrophys. J. **702**, 85 (2009).
[66]J. M. Brown, K. M. Pontoppidan, E. F. van Dishoeck, G. J. Herczerg, G. A. Blake, and A. Smette, Astrophys. J. **770**, 94 (2013).
[67]R. P. Hein Bertelsen, I. Kamp, M. Goto, G. van der Plas, W.-F. Thi, L. B. F. M. Waters, M. E. van den Ancker, and P. Woitke, Astron. Astrophys. **561**, A102 (2014).
[68]See supplementary material at http://dx.doi.org/10.1063/1.4958951 for a Fortran subroutine to generate the V6D PES.

Reuse of AIP Publishing content is subject to the terms: https://publishing.aip.org/authors/rights-and-permissions. Downloaded to IP: 128.118.81.59 On: Wed, 23 Nov 2016 20:49:22